Pump-Probe Spectroscopy with Entangled Photons

P. Munkhbaatar[1],* K. Myung-Whun[2,3], and D. Ulam-Orgikh[1]
[1]*Department of Physics, School of Science, NUM, Ulaanbaatar 210646, Mongolia*
[2]*Department of Physics, CNU, 561-756 Jeon-ju, Korea*
[3]*Institute of Photonics and Information Technology, CNU, 561-756 Jeon-ju, Korea*

A pump-probe spectroscopy using polarization controlled entangled photons was proposed to improve the spectral resolution of optical signals in solids. Numerical simulation showed that stimulated Raman scattering response due to simple phonon and phonon coupled to orbital excitation can be discriminated in transmittance signal of a small cluster system mimicking $LaMnO_3$, a Mott insulator with orbital ordering. The simulation showed that orthogonal polarizations of the pump and probe light field suppressed the simple phonon peaks, while it could not suppress the phonons coupled to orbital excitation.

PACS numbers: 42.25.Ja, 78.47.J-, 42.50.Ct

I. INTRODUCTION

Light-matter interactions can provoke optical excitations between the quantum states of the matter, which result into distinguishable features in infrared and Raman spectra. Analysis of the spectral features provides the information of the interactions in the many-body quantum states of the matter[1]. In some solid matters such as strongly correlated electron systems, however lattice, charge, spin and orbital degree of freedom compete each other on similar energy scales to form the complicated low energy states[2], so numerous possibilities are allowed for optical excitations of microscopically different origins at similar energy scales, which causes ambiguity in the interpretation of the spectral features[3–6].

The ambiguity can be reduced, if multiple light fields are employed as proposed in some non-linear optical techniques[7]. Amplitude of the optical signal is proportional to the expectation values of the dipole operator acted upon the energy eigen-states of the matter. When the multiple light fields are used, numerous combinations of the light field creation or annihilation operators are involved in the light-matter interaction process in the experiment. Combinations of light fields with different frequencies allow the optical processes for different excitation-decay paths, which makes the intensity signals of the processes to appear at different places in the multi-dimensional frequency space composed of those light field frequencies. More information of the light-matter interaction process thus can be obtained from the multi-dimensional spectra[8]. Furthermore if those multiple light fields are entangled by their frequencies, fine tuning of the interference between the entangled light fields can make signal intensities of different excitation-decay paths to be different, which provides the chances to discriminate the light-matter interaction processes less ambiguously from the optical spectra[9].

Entangled-light-field spectroscopic methods therefore may have advantage to resolve the low energy quantum states of the strongly correlated electron solid matter systems. However, application of the methods to the strongly correlated systems has not been an issue of particular concern so far. It is probably because the optical signals in those systems have bandwidth usually comparable or broader than the minute energy differences between the subband peaks formed by the emission or absorption of phonon, magnon, or orbiton for the optical processes. The signal intensity differences provided by the entangled-light-field spectroscopic methods may not be significant enough to distinguish the smeared and overlapped neighboring peaks. In this paper, we suggest that optical pump-probe method using polarization controlled entangled-photon pairs can be used to distinguish optical excitations of which resonant energy is very similar but the microscopic light-matter interaction process is quite different in a model system. For the demonstration, we numerically simulated the polarization dependence of the entangled-photon pump-probe response of a Mott insulator of which geometrical symmetry of the valence orbitals was broken.

II. MODEL AND METHOD

A. Hamiltonian

We choose $LaMnO_3$ as a model material system. This material system is well known for the spin and orbital ordering[2]. $LaMnO_3$ has Mn^{3+} ions with electronic configuration $3d^4$ in high-spin state. Here one electron occupies one of the doubly degenerate valence orbitals. The orbitals show $3x^2-r^2/3y^2-r^2$ type ordering coupled to the JT lattice distortion

*Electronic address: p_munhkbaatar@yahoo.com

and the spins show A-type ordering in the ground state. To mimic one lattice layer of the orbital and spin ordered $LaMnO_3$ crystal, we built an ideal Mn-cluster composed of four Mn^{3+} ions[10]. The Hamiltonian of the system was built based on a quasi-two-dimensional two-orbital Hubbard model as follows:

$$\begin{aligned} H &= t(c^{\dagger}_{1,3x^2-r^2}c_{2,3x^2-r^2} + c^{\dagger}_{4,3x^2-r^2}c_{3,3x^2-r^2} + c^{\dagger}_{1,3y^2-r^2}c_{4,3y^2-r^2} + c^{\dagger}_{2,3y^2-r^2}c_{3,3y^2-r^2} + h.c) \\ &+ U\sum_i n_{i,3z^2-r^2}n_{i,x^2-y^2} + \omega_(ph)b^{\dagger}b + q(b^{\dagger}+b)\sum_i (-1)^i T^x_i + Q_3\sum_i T^z_i + \sum_{(i,j)} J_\gamma T^\gamma_i \langle T^\gamma_j\rangle. \end{aligned} \quad (1)$$

Here the first term was kinetic energy of Mn ion e_g electron, t was the hopping integral between neighboring Mn sites. $c^{\dagger}_{i\alpha}$ ($c_{i\alpha}$) represented the electron creation (annihilation) operator with orbital α at site i. $3x^2-r^2$ (and $3y^2-r^2$) represented the spatial symmetry of Mn electron orbital α. The second term was the on-site Coulomb interaction. U was the Coulomb repulsion energy between two electrons occupying different e_g orbitals of the same Mn site with high spin configuration. The third term was Q_2-type JT phonon contribution. ω_{ph} was the Q_2 phonon energy and $b^{\dagger}$ (b) was the phonon creation (annihilation) operator. The fourth term was the electron-phonon interaction. q was the electron-phonon coupling constant and T^{α}_i was the localized orbital pseudo-spin operator. The fifth term was Q_3-type static JT distortion. Last term was the super-exchange interaction between the orbitals in the four-Mn-cluster and the outside orbitals surrounding the cluster. We solved the Hamiltonian numerically to find the eigenvalues and the eigen-states[10]. Fig.1(a) shows the energy eigen-states schematically. $|g\rangle$ represented a set of eigen-states, i.e. $|g_1\rangle, |g_2\rangle, ...$ which included the ground state $|g_1\rangle$. Double occupation of electrons at one Mn-site e_g orbitals was not allowed for those states. The energy difference between $|g_n\rangle$ and $|g_{n+1}\rangle$ was due to the phonon-orbital coupling energy difference for different octahedral distortion and orbital ordering configuration. Second set, $|e\rangle = |e_1\rangle, |e_2\rangle, ...$ represented the set of photo-excited eigen-states. The excited state denoted one hole and one double occupation. One element of the set can be represented schematically as $\left|\begin{matrix}\uparrow & \downarrow \\ 0 & \uparrow\downarrow\end{matrix}\right\rangle$, for example. Here the arrows depict the pseudo-spin (i.e. orbital) state of a Mn-site in the cluster. The energy difference between $|g_n\rangle$ and $|e_n\rangle$ was mainly due to Coulomb energy (U). The energy difference between $|e_n\rangle$ and $|e_{n+1}\rangle$ was due to phonon-orbital coupling between the sites similar as in $|g_n\rangle$. Third set of higher energy ($\sim 2U$) photo-excited states, $|f\rangle$ (not shown in Fig.1(a)) can be also considered in the interaction process. This set corresponded to the two doubly occupied states which can be represented schematically as $\left|\begin{matrix}\uparrow\downarrow & 0 \\ 0 & \uparrow\downarrow\end{matrix}\right\rangle$.

B. Formalism of pump-probe signal

Here, the calculation procedure was briefly explained. Details of the method can be found in Refs.[9, 13]. ($\vec{k}_1$, ω_1) mode as the pump light mode and ($\vec{k}_2$, ω_2) mode as the probe mode was considered. The frequency domain PP signal with quantum optical modes ($S(\omega_1, \omega_2)$) was defined as $S(\omega_1, \omega_2) = T(\omega_1, \omega_2)_{with} - T(\omega_2)_{without}$. $T(\omega_1, \omega_2)_{with}$ indicated the transmittance intensity of probe light signal measured with pump light mode illumination and $T(\omega_2)_{without}$ indicated the transmittance intensity of probe light signal measured without pump light mode illumination. The PP signal was calculated as $P^{(3)}$ (third order polarization) in the probe mode direction. The probe mode direction was $\vec{k}_1 - \vec{k}_1 + \vec{k}_2$ because of the phase matching condition. Note that the phase matching condition was considered in the free space.

The nonlinear polarization was induced by the sequence of interactions with the optical fields. When the last interaction occurs with the $\vec{k}_2$ mode, it generated $P^{(3)}(\vec{k}_2, t)$. Thus, the signal was defined as following:

$$S(\omega_1, \omega_2) = -\,\mathrm{Im}\left[\frac{1}{T}\int_{-T}^{T} dt \left\langle \varepsilon_2^{\dagger}(t) P^{(3)}(\vec{k}_2, t)\right\rangle\right] \quad (2)$$

Here $\varepsilon_2^{\dagger}(t)$ was the negative frequency component of the probe mode, and $2T$ was the measurement time [10]. In the rotating wave approximation (RWA), the matter-field coupling was given by

$$H_{int}(t) = \mu^{\dagger}(t)\varepsilon(t) + \mu(t)\varepsilon^{\dagger}(t). \quad (3)$$

Here the dipole operator was partitioned as $\mu^{\dagger}(t) + \mu(t)$, where

$$\mu(t) = \sum_{k>l} \mu_{lk} e^{-i(E_k - E_l)t} |l\rangle\langle k| \quad (4)$$

was the positive frequency part and it represented the transition from the higher energy state to lower energy state; $\{|k\rangle\}$ represented the energy eigenstates of the four-Mn-cluster system. $\mu^\dagger$ represented the transition from the lower energy state to the higher energy state.

The field of mode $\varepsilon_j(t)$ $(j = 1, 2)$ was similarly partitioned as $\varepsilon(t) + \varepsilon^\dagger(t)$, where the positive frequency component was

$$\varepsilon_j(t) = \left(\frac{2\pi\omega_j}{\Omega}\right)^{(1/2)} a_j e^{-i\omega_j t}. \quad (5)$$

Here, a_j $(a_j^\dagger)$ was the annihilation (creation) boson operator for the j-th mode and Ω was the quantization volume.

Using the super-operator non-equilibrium Green's function (SNGF) formalism [9] and the eight close-time-path-loop (CTPL) diagrams, Eq.(2) can be expressed in terms of four-point correlation function of the matter and the field as follows:

$$\begin{aligned} S(\omega_1,\omega_2) &= -\,\mathrm{Im}\Big\{\langle\mu G^\dagger(\omega_1)\mu G^\dagger(\omega_1+\omega_2)\mu^\dagger G(\omega_1)\mu^\dagger\rangle\langle a_1^\dagger a_2^\dagger a_2 a_1\rangle + \langle\mu G^\dagger(\omega_2)\mu G^\dagger(\omega_2+\omega_1)\mu^\dagger G(\omega_1)\mu^\dagger\rangle\langle a_2^\dagger a_1^\dagger a_2 a_1\rangle \\ &+ \langle\mu G^\dagger(\omega_1)\mu G^\dagger(\omega_1+\omega_2)\mu^\dagger G^\dagger(\omega_2)\mu^\dagger\rangle\langle a_1^\dagger a_2^\dagger a_1 a_2\rangle + \langle\mu G^\dagger(\omega_2)\mu G^\dagger(\omega_1+\omega_2)\mu^\dagger G^\dagger(\omega_2)\mu^\dagger\rangle\langle a_2^\dagger a_1^\dagger a_1 a_2\rangle \\ &+ \langle\mu G^\dagger(\omega_2)\mu^\dagger G(0)\mu G(\omega_1)\mu^\dagger\rangle\langle a_2^\dagger a_2 a_1^\dagger a_1\rangle + langle\mu G^\dagger(\omega_1)\mu^\dagger G(\omega_1-\omega_2)\mu G(\omega_1)\mu^\dagger\rangle\langle a_1^\dagger a_2 a_2^\dagger a_1\rangle \\ &+ \langle\mu G^\dagger(\omega_1)\mu^\dagger G^\dagger(0)\mu G^\dagger(\omega_2)\mu^\dagger\rangle\langle a_1^\dagger a_1 a_2^\dagger a_2\rangle + \langle\mu G^\dagger(\omega_2)\mu^\dagger G^\dagger(\omega_2-\omega_1)\mu G^\dagger(\omega_2)\mu^\dagger\rangle\langle a_2^\dagger a_1 a_1^\dagger a_2\rangle\Big\}. \quad (6) \end{aligned}$$

Here $G(\omega) = (\omega + E_{g_1} - H + i\gamma)^{-1}$. The eight terms in Eq.(6) corresponded to the eight diagrams of Fig. 4 in Ref.[9]. The interactions were time ordered within each branch of the diagram, but the two branches were not time ordered with respect to each other. By convention, the chronologically last interaction was absorption and it occurred at the left branch of the loop.

C. Pump-probe spectroscopy with entangled photons

It is proposed that the PP process carried out with two entangled optical modes. Original method was proposed by Roslyak to selectively investigate quantum pathways in the PP response of non-interacting molecules [9, 11]. In the proposed PP spectroscopy, the pump and the probe optical modes were produced by the parametric down conversion process (PDC) in a nonlinear optical crystal such as $BaBO_2$. External excitation light with frequency ω_{ex} and the wave-vector $\vec{k}_{ex}$ illuminates the nonlinear crystal, then two entangled optical modes (wave-vector $\vec{k}_1$, $\vec{k}_2$ and frequency ω_1, ω_2 respectively) were created. Due to the phase matching condition, the frequency (wave-vector) of the external excitation light and the two entangled optical modes should satisfy $\omega_{ex} = \omega_1 + \omega_2$ $(\vec{k}_{ex} = \vec{k}_1 + \vec{k}_2)$. Note that the phase matching condition was considered inside of the nonlinear crystal. In the free space the value and the direction of the wave-vectors can be different because of the refraction.

Let't assume that our model system, i.e. the four-Mn-cluster interact with two entangled optical modes such as ($\vec{k}_1$, ω_1) mode as the pump light mode and ($\vec{k}_2$, ω_2) mode as the probe mode. Then the PP signal was generated by the change in the absorption of ($\vec{k}_2$, ω_2) mode due to the interaction of our model system with ($\vec{k}_1$, ω_1) mode. The arrival time of ($\vec{k}_2$, ω_2) mode and that of ($\vec{k}_1$, ω_1) mode on the sample were not well separated because of the same path length. We added a small modification, a half-wave plate (or periscope) to Roslyak's original idea for the polarization control of the pump light mode. Schematic diagram of the proposed setup was shown in Fig. 1(b).

Nonlinear optical processes can be generated by many optical modes. Those processes can be described by the CTPL diagrams [13]. We interested in only the PP process, which can be represented by the sum of eight CTPL diagrams according to the RWA [9, 13]. The CTPL diagrams are called as the transition pathways. More detail explanation of PP signal is given in pervious section. According to Roslyak, the pathways can be divided into two groups if three-energy-level system in the non-interacting atomic limit is involved in the PP process. In the first group, the pathways showed that the system evolves from the ground state (g) to an excited state (e) by absorbing an optical mode, then to another excited (f) by absorbing one more optical mode, and to a lower energy excited state (e) by emitting an optical mode, then finally to the ground state (g) by emitting an optical mode, which can be represented

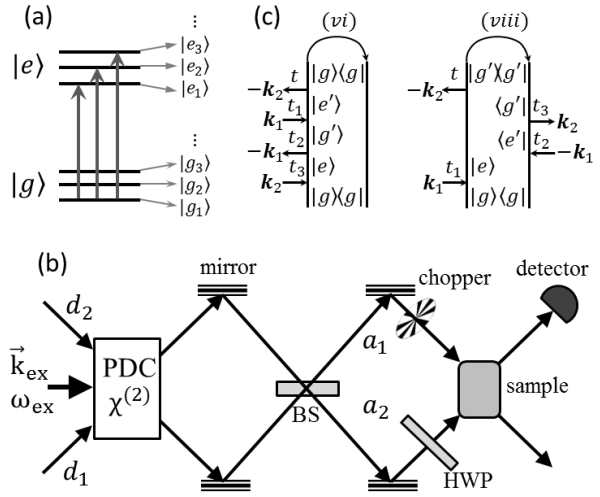

Зурар 1: (a) Schematic energy level diagram. (b) Schematic experimental setup for the pump-probe method with entangled photons. PDC was a nonlinear crystal used to obtain entangled-photon pairs from the classical external excitation beam by parametric down conversion. BS was 50:50 beam splitter. HWP (half wave plate) was used to control the polarization of $\vec{k}_1$ mode. The detector measured the photon flux in $\vec{k}_2$ mode. d_1 and d_2 were annihilation operators for the original non-entangled (canonical) modes and a_1, a_2 represent the entangled modes. (c) Loop diagrams representing the entangled photon-matter quantum pathways contributing to pump-probe signal with weak external excitation field.

shortly by $g \to e \to f \to e \to g$. All of these pathways were multiplied by the optical field correlation functions of the form $\langle a^\dagger a^\dagger a a\rangle$, where $a(a^\dagger)$ was the annihilation (creation) of the optical modes [9]. This group is called as two-photon absorption (TPA). In the second group, the system undergoes back and forth single photon absorption and emission, and the pathway can be described by $g \to e \to g \to e \to g$. This process or group is called as stimulated Raman-Scattering (SRS). All of these pathways were multiplied by the optical field correlation functions of the form $\langle a^\dagger a a^\dagger a\rangle$ [9].

In case of conventional PP experiments, optical correlation functions of the form $\langle a^\dagger a^\dagger a a\rangle$ and $\langle a^\dagger a a^\dagger a\rangle$ yields all identical response. Because the light fields are treated as the classical optical modes. Therefore optical correlation functions of the form $\langle a^\dagger a^\dagger a a\rangle$ and $\langle a^\dagger a a^\dagger a\rangle$ pathways are all summed together, hence TPA and SRS become indistinguishable.

On the other hand, the PP method with entangled optical modes can discriminate those pathways selectively as Roslyak *et al.* pointed [9]. It is because the optical correlation functions can have different signal intensity for different pathways. Let us look into the proposed setup shown in Fig. 1(b). Pair of photons was generated by the PDC process and they illuminate the sample. The photon fields for the pump light can be described by $a_1(a_1^\dagger)$ and the photon fields for the probe light can be described by $a_2(a_2^\dagger)$. a_1 and a_2 fields can be transformed from the vacuum fields (d_1 and d_2) with the conversion coefficients $U = \cosh G$ and $V = -i \sinh G$ as follows;

$$\begin{aligned} a_1 &= \frac{1}{\sqrt{2}}[(Ud_1 + Vd_2^\dagger) + i(Ud_2 + Vd_1^\dagger)], \\ a_2 &= \frac{1}{\sqrt{2}}[i(Ud_1 + Vd_2^\dagger) - (Ud_2 + Vd_1^\dagger)]. \end{aligned} \quad (7)$$

Here G represented the single-pass gain of the conversion process and it can be written as $G = g|\varepsilon_{ex}|L$, where g was a gain coefficient proportional to the second-order susceptibility $\chi^{(2)}$ of the nonlinear crystal, ε_{ex} was the amplitude of the external excitation field, and L was the interaction path length. i was $\sqrt{-1}$. More details of the operator representation of the method can be found in Ref.[14].

The PP experiment was conducted with these transformed fields a_1 and a_2. For the first group of pathways (TPA), the optical field correlation function can be simplified into the following forms according to Roslyak *et al.* [9]:

$$\begin{aligned} \langle a_1^\dagger a_2^\dagger a_2 a_1\rangle &= \langle a_1^\dagger a_2^\dagger a_1 a_2\rangle = \langle a_2^\dagger a_1^\dagger a_2 a_1\rangle \\ &= \langle a_2^\dagger a_1^\dagger a_1 a_2\rangle = V^4 \end{aligned} \quad (8)$$

The second group (SRS) has different forms. Among eight pathways counted by Roslyak *et al.* [9], only the fifth (v), sixth (vi), seventh (vii), and the eight ($viii$) are belong to the second group. The fifth (v) and seventh (vii) pathways have the following forms,

$$\langle a_1^\dagger a_1 a_2^\dagger a_2\rangle = \langle a_2^\dagger a_2 a_1^\dagger a_1\rangle = V^4. \quad (9)$$

The sixth (vi) and eight ($viii$) pathways have the following forms,

$$\langle a_1^\dagger a_2 a_2^\dagger a_1\rangle = \langle a_2^\dagger a_1 a_1^\dagger a_2\rangle = V^2 + V^4. \quad (10)$$

The pathways were shown in Fig.1(c) for which the CTPL diagrams of Marx *et al.* were adopted [**?**]. Note that therefore at low excitation intensity, the intensity square term will be much weaker than the intensity term, i.e. $V^2 \gg V^4$ (V^2 corresponds to the external excitation light intensity). In this limit the contribution of pathways of Eqs.(8) and (9) can be neglected. The PP signal therefore will be given solely by (vi) and ($viii$) pathways shown in Fig.1(c), and it can be given by following equation;

$$S^{(Ent)}(\omega_1, \omega_2) \sim |\varepsilon_{ex}|^2 \,\mathrm{Im}[\chi^{(vi)}(\omega_1, \omega_2) + \chi^{(viii)}(\omega_1, \omega_2)]. \quad (11)$$

For the derivation of the equation, see Eq.(6) in pervious section. Eq.(6) can be simplified into

Eq.(11), $S^{(ent)}(\omega_1,\omega_2)$ by considering only (vi) and $(viii)$ pathways. To get this PP signal in the experiment, one need to measure the probe signal only by blocking the pump light, then subtract this signal from the probe signal with the pump light illumination.

D. Numerical simulation for the pump-probe signal with energy eigen-states

The PP signal of Eq. (11) was the sum of two pathways contributions. The third order susceptibilities of the pathways were given by

$$\chi^{(vi)}(\omega_1,\omega_2)=\sum_e\sum_{g'}\sum_{e'}\mu^{\beta}_{g_1e'}\mu^{\alpha}_{e'g'}\mu^{\alpha}_{g'e}\mu^{\beta}_{eg_1}I_{eg_1}(\omega_2)I_{g'g_1}(\omega_2-\omega_1)I_{e'g_1}(\omega_2), \tag{12}$$

$$\chi^{(vi)}(\omega_1,\omega_2)=\sum_e\sum_{g'}\sum_{e'}\mu^{\alpha}_{g_1e'}\mu^{\beta}_{e'g'}\mu^{\beta}_{g'e}\mu^{\alpha}_{eg_1}I_{eg_1}(\omega_1)I^{*}_{g'g_1}(\omega_1-\omega_2)I^{*}_{e'g_1}(\omega_1). \tag{13}$$

Here $\mu^{\alpha,\beta}_{eg}$ was the dipole matrix element between two energy eigen-states $|e\rangle$ and $|g\rangle$ of the full Hamiltonian (H), i.e $\langle e|\vec{r}|g\rangle$. $\vec{r}$ was the dipole displacement operator. The superscripts α and β indicated the polarization direction of a_1 (pump) and a_2 (probe) modes, respectively. $I_{eg}(\omega)$ was the auxiliary function;

$$I_{eg}(\omega)=1/(\omega-(E_e-E_g)+i\gamma). \tag{14}$$

E_e was the energy or eigen-value of $|e\rangle$. γ was the dephasing rate which was equal to the phenomenological spectral broadening parameter [9]. To obtain the dipole matrix element, I used the current operator $\vec{j}$. $\vec{r}|g\rangle$ was obtained by solving $\vec{j}|g\rangle=i(H-E_g)\vec{r}|g\rangle$. Therefore the current operator $\vec{j}$ and the dipole operator $\vec{\mu}$ should satisfy the following relations:

$$j^{\alpha,\beta}=-i[\mu^{\alpha,\beta},H],\mu^{\alpha,\beta}_{eg}=ij^{\alpha,\beta}_{eg}/(E_e-E_g). \tag{15}$$

[ ] represented the commutation relation [14]. $j=it\sum_{(n,m)_\alpha}(c^{\dagger}_{n,\sigma}c_{m,\sigma}-h.c.)$. For $\alpha=x$, $\sigma=3x^2-r^2$. For $\alpha=y$, $\sigma=3y^2-r^2$. n,m represented the nearest neighboring Mn-ion site index of the four-Mn-cluster. This allows us to calculate Eqs.(12) and (13) based on the energy eigen-states of the full Hamiltonian (H) given by Eq.(1).

III. RESULTS & DISCUSSION

The PP signal Eq.(11) were numerically obtained . Fig. 2 shows the calculated $S^{(Ent)}(\omega_1,\omega_2)$. Here the pump and probe polarizations were both parallel to a crystal axis. To see the contribution of each pathways, (vi) pathway contribution ($\mathrm{Im}[\chi^{(vi)}(\omega_1,\omega_2)]$) was shown in Fig. 2(a) and $(viii)$ pathway contribution ($\mathrm{Im}[\chi^{(viii)}(\omega_1,\omega_2)]$) was shown in Fig. 2(b).

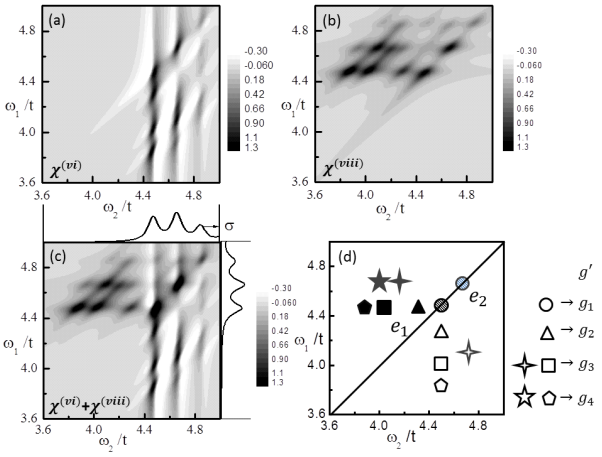

Зураг 2: The calculated transmittance intensity change, $T(\omega_1,\omega_2)$. Here the pump and probe polarizations were parallel. (a) $\mathrm{Im}[\chi^{(vi)}(\omega_1,\omega_2)]$ as function of ω_1 and ω_2, (b) $\mathrm{Im}[\chi^{(viii)}(\omega_1,\omega_2)]$ as function of ω_1 and ω_2 (c) sum of (a) and (b), and for comparison, $\sigma(\omega)$ were shown. (d) Summary of peaks observed in (a) and (b). Involved intermediate states were noted.

Fig. 2(a) shows the calculated (vi) pathway contributions. Here two clear peaks appeared along the diagonal line at $\omega_1=\omega_2=4.45t$ and at $\omega_1=\omega_2=4.65t$. These peaks were schematically represented as circles in Fig. 2(d). The $\omega_1=4.45t$ peak was due to the $g_1\rightarrow e_1\rightarrow g_1\rightarrow e_1\rightarrow g_1$ transition process, and the $\omega_1=4.65t$ peak was due to the $g_1\rightarrow e_2\rightarrow g_1\rightarrow e_2\rightarrow g_1$ process. There could be numerous available photo-excited states at higher energies. In our calculation, only the lowest optically active two excited states were regarded, and they were named as $|e_1\rangle$ and $|e_2\rangle$.

In addition to these peaks, three more peaks appeared along the vertical line at $\omega_2=4.45t$ and one more peak appeared along the vertical line at

$\omega_2 = 4.45t$. Former three peaks were due to the $g_1 \rightarrow e_1 \rightarrow g_n \rightarrow e_1 \rightarrow g_1$ transition processes. The peak at $\omega_1 = 4.3t$ corresponded to $n = 2$ transition, which was marked by an open triangle in Fig. 2(d). In this process, Q_2-type phonons can be generated according to our previous study. The strength of the peak indicates the transition probability between the ground state $|g_1\rangle$ and the quasi-ground state $|g_2\rangle$. If schematically described, $|g_2\rangle$ state was composed of the single-occupied Mn-ions and the collective vibration of MnO_6 octahedra. The width of the peak may be determined by the life time of the vibration, but in our calculation a phenomenological value $(0.05t)$ was used for all peaks in Fig. 2 and Fig. 3. The peak at $\omega_1 = 4.0t$ corresponded to $n = 3$ transition, which was marked by an open square in Fig. 2(d). Also in this process, Q_2-type phonons can be generated, however the phonons should be strongly coupled to the electron orbital occupations of every Mn ion. If schematically described, $|g_3\rangle$ state was composed of single-occupied Mn-ions and the collectively vibrating MnO_6 octahedra. The octahedral vibration frequency should be affected by the orbital occupation via JT interaction of the Mn-site. The peak at $\omega_1 = 3.8t$ corresponded to $n = 4$ transition, which was marked by an open pentagon in Fig. 2(d). In this process, Q_2-type phonons can be generated. However the phonons should be strongly coupled to the orbital occupations of every Mn ions via JT interaction, and they should be also coupled to the collective excitation of the ordered orbitals mediated by the SE interaction. If schematically described, $|g_3\rangle$ state was composed of single-occupied Mn-ions and the collectively vibrating MnO_6 octahedra which is coupled to the so-called orbital wave.

The latter peak along the vertical line at $\omega_2 = 4.65t$ was due to $g_1 \rightarrow e_2 \rightarrow g_n \rightarrow e_2 \rightarrow g_1$ transition processes. Here the peak at $\omega_1 = 4.25t$ corresponded to $n = 3$ transition, which was marked by an open star in Fig. 2(d). The peaks was produced by the similar process as that of the open square peak, but the intermediate state $|e_2\rangle$ may be more strongly coupled to the lattice degree of freedom than $|e_1\rangle$ state. $|e_1\rangle$ and $|e_2\rangle$ were nearly degenerate photo excited states, the energy difference between the states was due to their different empty-site and double occupied site configurations and the interaction of phonon and orbital degrees of freedom.

Fig. 2(b) shows the calculated (viii) pathway contributions. About five peaks appeared in addition to the two diagonal peaks. These peaks were schematically represented as solid symbols in Fig. 2(d). Peaks along the horizontal line at $\omega_1 = 4.45t$ were due to $g_1 \rightarrow e_1 \rightarrow g_n \rightarrow e_1 \rightarrow g_1$ transition process $(n = 2, 3, 4)$, and peaks along the horizontal line at $\omega_1 = 4.65t$ were due to the $g_1 \rightarrow e_2 \rightarrow g_n \rightarrow e_2 \rightarrow g_1$ process $(n = 3, 4)$.

Fig. 2(c) the sum of two pathways or

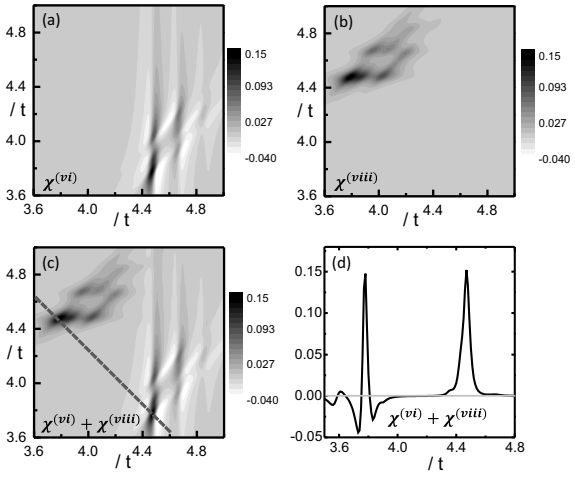

Зураг 3: The calculated transmittance intensity change, $T(\omega_1, \omega_2)$. Here the pump and probe polarizations were perpendicular. (a) $\mathrm{Im}[\chi^{(vi)}(\omega_1, \omega_2])$ as function of ω_1 and ω_2, (b) $\mathrm{Im}[\chi^{(viii)}(\omega_1, \omega_2)]$ as function of ω_1 and ω_2 (c) sum of (a) and (b). Dashed line represents the frequency phase matching condition (d) Off-diagonal cut of (c) along the dashed line, $S^{(en)}(\omega_1, \omega_{ex} - \omega_1)$.

$\mathrm{Im}[\chi^{(vi)}(\omega_1, \omega_2) + \chi^{(viii)}(\omega_1, \omega_2)]$. Beside of the panel, the linear optical conductivity, $\sigma(\omega)$ was presented for comparison (Here the spectral broadening was given by a phenomenological parameter $\gamma = 0.05t$). Peaks of $\sigma(\omega)$ were well matched to the diagonal peaks of $S^{(ent)}(\omega_1, \omega_2)$.

Fig. 3 shows the highlight point of our study. It provides basically the same signal, $\mathrm{Im}[\chi^{(vi)}(\omega_1, \omega_2)]$ and $\mathrm{Im}[\chi^{(viii)}(\omega_1, \omega_2)]$, but here the probe optical mode polarization was assumed to be orthogonal to that of the pump mode polarization. The orthogonal polarization configuration was achieved by the half-wave plate (or periscope) as shown in Fig. 1(c). The highlight point is that only a peak due to the $g_1 \rightarrow e_1 \rightarrow g_4 \rightarrow e_1 \rightarrow g_1$ transition process was clearly observed here and other peaks were suppressed. Note that $g_1 \rightarrow e_1 \rightarrow g_4 \rightarrow e_1 \rightarrow g_1$ transition process involves the phonon-coupled orbital wave excitation response. A part of the spectrum along the dashed line in Fig. 3(c) was presented in Fig. 3(d). This was $S^{(en)}(\omega_1, \omega_{ex} - \omega_1)$ for a fixed external excitation light field frequency (ω_{ex}). The line crossed the two phonon-coupled orbital wave signal peaks for $\chi^{(vi)}$ and $\chi^{(viii)}$. The peak for $\chi^{(vi)}$ was sharper than that for $\chi^{(viii)}$ and it showed the negative response. The negative response suggested that the transmittance of the system was enhanced (or absorption of the system was suppressed) by the pump light.

In real experiment, Fig. 2 and 3 can be obtained by measuring the spectral transmittance of the probe light mode signal. First the transmittance of the probe light should be measured by blocking the pump light illumination $(T(\omega_2)_{without})$. To get the

wavelength dependence, gratings and pinholes can be used. Then the transmittance of the probe light should be measured with the pump light illumination ($T(\omega_1, \omega_2)_{with}$). By subtracting the first signal from the second one, $S(\omega_1, \omega_2)$ can be obtained. This procedure can be simply and repeatedly done if an optical chopper and a lock-in amplifier were combined. The chopper can block and pass the pump light repeatedly in a fixed frequency, the lock-in amplifier can pick up the given frequency signal only. $S(\omega_1, \omega_2)$ can be estimated from the signal; for example, photo-voltage increase (or decrease) with respect to the background corresponds to the signal. Also the gratings and pinholes cab be used to select a specific wavelength components, but they should be correctly arranged to meet the phase matching condition ($\omega_{ex} = \omega_1 + \omega_2$ and $\vec{k}_{ex} = \vec{k}_1 + \vec{k}_2$)[12].

In present study, spontaneous parametric down conversion process was considered for the pump and probe light fields preparation. In the process, the generated light fields are quite weak, so it may be difficult to get clear signals. Intense light fields can be produced by parametric amplification process. Although the detailed nature of the quantum correlations can be quite different for parametric down conversion and for parametric amplification, quantum state signatures of light used in this study can remain also for intense light fields generated by the parametric amplification process as Nagasako *et al.* observed [14]. It means that we can expect the same results as predicted in Fig. 2 and 3 for the measurement used the parametric amplification process for pump and probe light sources. Also if broader band light source can be used for the external excitation light, more spectral information can be achieved. Ultra-short laser pulse can be used as the light source for such purpose, and further theoretical studies using pulse light source are demanded.

Finally, it should be noted that Fig. 3 implies the promising advantages of the proposed method. Note that in Fig. 3 only peaks corresponding to $g_1 \rightarrow e_1 \rightarrow g_4 \rightarrow e_1 \rightarrow g_1$ process (phonon-coupled orbital wave excitation) were shown and other peaks were suppressed. If the phonon-coupled orbital wave exists in reality, application of the addition external perturbation will reveal the different aspects of the orbital wave. In many optical experiments including the conventional PP method, the application of external perturbations such as magnetic field and hydrostatic pressure may change not only the optical response of the phonon-coupled orbital wave but also the other responses including the Mott gap excitation and the simple phonons. If the proposed method can be employed, it may have the capability to separate the phonon-coupled orbital wave signal from other responses clearly even under the magnetic field and hydrostatic pressure.

IV. CONCLUSION

A PP spectroscopy method with entangled photons was proposed to investigate the low energy collective excitations of $LaMnO_3$ theoretically. $LaMnO_3$ may have a few low energy collective excitations of which microscopic origins are different. Among them, the phonon-coupled orbital wave is interesting, but it was difficult to separate this mode from other excitation modes. With the proposed method, by controlling the degree of entanglement of incoming photon pairs, it is shown that phonon-coupled orbital wave mode can be selected clearly. This powerful method can be used to study the orbital wave of $LaMnO_3$, but it can be also used to investigate the collective excitations in many other strongly correlated electron systems.

[1] D. N. Basov, R. D. Averitt, D. V. Marel, M. Dressel, and K. Haule, Rev. Mod. Phys. **83**, 471 (2011).

[2] Y. Tokura, and N. Nagaosa, Science 288, 462 (2000).

[3] E. Saitoh, S. Okamoto, K. T. Takahashi, K. Yamamoto, T. Kimura, S. Ishihara, S. Maekawa, and Y. Tokura, Nature **410**, 180 (2001); E. Saitoh, S. Okamoto, K. Tobe, K. Yamamoto, T. Kimura, S. Ishihara, S. Maekawa, and Y. Tokura, Nature **418**, 40 (2002)

[4] M. Grüninger, R. Rückamp, M. Windt, P. Reutler , C. Zobel, T. Lorenz, A. Freimuth, and A. Revcolevschi, Nature **418**, 39 (2002).

[5] Jeroen van den Brink, Phys. Rev. Lett. **87**, 217202 (2001).

[6] M. W. Kim, P. Murugavel, S. Parashar, J. S. Lee, and T. W. Noh, New J. Phys. **6**, 156 (2004).

[7] S. Mukamel, Principles of Nonlinear Optical Spectroscopy (Oxford University Press, New York, 1995).

[8] P. Hamm, M. H. Lim, and R. M. Hochstrasser, J. Phys. Chem. **B 102**, 6123 (1998).

[9] O. Roslyak, C. Marx, and S. Mukamel, Phys. Rev. **A 79**, 033832 (2009)

[10] P. Munkhbaatar, and K. Myung-Whun, J. Mod. Opt. **61**, 197 (2014).

[11] O. Roslyak, and S. Mukamel, Phys. Rev. **A 79**, 063409 (2009).

[12] The phase matching condition was considered inside the nonlinear crystal. In free space the magnitude and the direction of the wave-vectors can be different because of the refraction.

[13] C. A. Marx, U. Harbola, and S. Mukamel, Phys. Rev. **A 77**, 022110 (2008).

[14] E. M. Nagasako, S. J. Bentley, R. W. Boyd, and G.

S. Agarwal, Phys. Rev. **A 64**, 043802 (2001).